Journal of Cellular Physiology

Actin binding LIM 1 (abLIM1) negatively controls osteoclastogenesis by regulating cell migration and fusion

Journal:	*Journal of Cellular Physiology*
Manuscript ID	JCP-17-0816.R2
Wiley - Manuscript type:	Original Research Article
Date Submitted by the Author:	14-Mar-2018
Complete List of Authors:	Narahara, Haruna; Nagasaki Daigaku Sakai, Eiko; Nagasaki University Graduate School of Biomedical Sciences Yamaguchi, Yu ; Nagasaki University Graduate School of Biomedical Sciences Narahara, Shun; Nagasaki University Graduate School of Biomedical Sciences Iwatake, Mayumi; Nagasaki University, Basic and Translational Research Center for Hard Tissue Disease Yoshida, Noriaki; Nagasaki University Graduate School of Biomedical Sciences, Division of Orthodontics and Dentofacial Orthopedics Tsukuba, Takayuki; Nagasaki University Graduate School of Biomedical Sciences, Department of Dental Pharmacology,
Key Words:	abLIM1, osteoclastogenesis, cell migration, cell fusion, actin formation

Actin binding LIM 1 (abLIM1) negatively controls osteoclastogenesis by regulating cell migration and fusion

Haruna Narahara[1, 2], Eiko Sakai[1], Yu Yamaguchi[1], Shun Narahara[1], Mayumi Iwatake[1, 3], Kuniaki Okamoto[1, 4], Noriaki Yoshida[2], and Takayuki Tsukuba[1*]

[1]Department of Dental Pharmacology, Graduate School of Biomedical Sciences, Nagasaki University, Nagasaki 852-8588, Japan

[2]Department of Orthodontics and Dentofacial Orthopedics, Graduate School of Biomedical Sciences, Nagasaki University, Nagasaki 852-8588, Japan

Present address:[3]Basic and Translational Research Center for Hard Tissue Disease, Graduate School of Biomedical Sciences, Nagasaki University, Nagasaki 852-8588, Japan

Present address: [4]Department of Dental Pharmacology, Okayama University Graduate School of Medicine, Dentistry and Pharmaceutical Sciences, Okayama, 700-8525

Running title: abLIM1 controls osteoclastogenesis

[*]To whom correspondence should be addressed:

Dr. Takayuki Tsukuba, Department of Dental Pharmacology, Graduate School of Biomedical Sciences, Nagasaki University, Nagasaki 852-8588, Japan.

Tel. 81-92-642-6337; Fax 81-92-642-6342; E-mail: tsuta@nagasaki-u.ac.jp

Keywords: abLIM1, osteoclastogenesis, cell migration, cell fusion, actin formation

Abstract

Actin binding LIM 1 (abLIM1) is a cytoskeletal actin-binding protein that has been implicated in interactions between actin filaments and cytoplasmic targets. Previous biochemical and cytochemical studies have shown that abLIM1 interacts and co-localizes with F-actin in the retina and muscle. However, whether abLIM1 regulates osteoclast differentiation has not yet been elucidated. In this study, we examined the role of abLIM1 in osteoclast differentiation and function. We found that abLIM1 expression was upregulated during receptor activator of nuclear factor kappa-B ligand (RANKL)-induced osteoclast differentiation, and that a novel transcript of abLIM1 was exclusively expressed in osteoclasts. Overexpression of abLIM1 in the murine monocytic cell line, RAW-D suppressed osteoclast differentiation and decreased expression of several osteoclast-marker genes. By contrast, small interfering RNA-induced knockdown of abLIM1 enhanced the formation of multinucleated osteoclasts and markedly increased the expression of the osteoclast-marker genes. Mechanistically, abLIM1 regulated the localization of tubulin, migration, and fusion in osteoclasts. Thus, these results indicate that abLIM1 negatively controls osteoclast differentiation by regulating cell migration and fusion mediated via actin formation.

Introduction

Actin binding LIM 1 (abLIM1) is a cytoskeletal actin-binding protein that encodes a LIM zinc-binding domain at the N-terminus and dematin-like domain at the C-terminus. abLIM1 was initially discovered as a protein homologous to dematin that mediates interactions between actin filaments and cytoplasmic targets (Kim et al., 1997; Roof et al., 1997). Studies using cDNA libraries revealed that abLIM1 is mainly distributed as three distinct isoforms: abLIM1-L (long), abLIM1-M (middle), and abLIM1-S (short), respectively (Roof et al., 1997). Moreover, the findings that abLIM1 biochemically interacts with F-actin, and cytochemically co-localizes with F-actin in the retina indicate that abLIM1 possibly regulates the actin cytoskeleton in the retina (Roof et al., 1997). However, abLIM1-L knockout mice have been shown to display no phenotypes of retinal development and maturation, suggesting that abLIM1-L is not essential for retinal development (Lu et al., 2003). Subsequently, a genetic study involving humans has shown abnormal splicing of abLIM1 in the skeletal muscles of patients with myotonic dystrophy type 1, which is characterized by muscle weakness and cardiac defects (Ohsawa et al., 2015). Although abLIM1 is probably involved in the regulation of actin cytoskeleton in mammalian cells, the physiological role of abLIM1 has not been elucidated. Here, we demonstrate the role of abLIM1 in osteoclasts.

Osteoclasts are bone resorbing giant cells that have multinucleated formations (Teitelbaum, 2000). The multinucleations are formed by the fusion of mononuclear progenitors of the monocyte/macrophage lineage (Boyle et al., 2003). This process is strictly controlled by various factors. Initially, stimulation of mononuclear progenitors with the essential differentiation cytokines [macrophage colony-stimulating factor (M-CSF) and receptor activator of nuclear factor kappa-B ligand (RANKL)] induces release of

chemokines, including CXCL12 (stromal cell-derived factor-1), CX3CL1 (fractalkine), and related molecules that are activated around other precursor cells (Ishii et al., 2010). Subsequently, these chemokines enhance migration and aggregation of cells adjacent to the secreted cells (Kikuta and Ishii, 2013). Finally, the aggregated cells undergo cell-cell fusion through the key molecules on the plasma membrane, including DC-STAMP, SIRP-a/CD47, and E-cadherin (Fiorino and Harrison, 2016; Lundberg et al., 2007; Yagi et al., 2006). In particular, DC-STAMP-deficient osteoclast-precursor cells lack multinucleation owning to cell-cell fusion defects (Yagi et al., 2005). Recently, it has been proposed that actin-mediated cell extension formation of pre-osteoclasts termed as "fusopods" is essential for the cell fusion process of osteoclast differentiation (Wang et al., 2015). Although regulation of the actin cytoskeleton is important for polarization, adhesion, and migration of osteoclasts, the mechanisms by which actin mediates the regulation of osteoclasts remain largely unknown.

To explore these mechanisms, we conducted DNA microarray analysis, which indicated that 1,363 genes were upregulated and 881 genes were downregulated during osteoclastogenesis (Shimada-Sugawara et al., 2015). During a series of experiments involving osteoclasts, we found abLIM1 to be an upregulated gene. In this study, by using transfection of small interfering RNA (siRNA) transfection or gene overexpression systems, we demonstrated that abLIM1 negatively regulates osteoclast differentiation of mouse macrophage-like RAW-D cells or bone-marrow macrophages (BMMs).

Materials and Methods

Reagents

Alpha-minimum essential medium (α-MEM) was purchased from WAKO (Osaka, Japan). Fetal bovine serum (FBS) was obtained from Sigma-Aldrich (St. Louis, MO, USA). Recombinant RANKL was prepared as described previously (Sakai et al., 2012). Anti-cathepsin K antibody was prepared as previously described (Kamiya et al., 1998). Macrophage colony-stimulating factor (M-CSF) was purchased from Kyowa Hakko Kogyo (Tokyo, Japan). Polyclonal antibodies were purchased as follows: anti-GAPDH antibody (Cat.No. 5174S, D16H11) was purchased from Cell Signaling Technology (Danvers, MA, USA; all rabbit); anti-α-tubulin antibody was from Santa Cruz Biotechnology (CA, USA); anti-Src antibody were from Merck Millipore (Darmstadt, Germany; Cat.No. 05-184, clone GD11); anti-abLIM1 antibody was from Proteintec Inc. (15129-1-AP, Tokyo, Japan). Osteo Assay Plates were purchased from Corning (Corning, NY, USA). All other reagents, including phenylmethylsulfonyl fluoride, and the protease inhibitor cocktail were obtained from Sigma-Aldrich.

Cell culture

Murine monocytic cell line RAW-D cells were kindly provided by Prof. Toshio Kukita (Kyushu University, Japan) as previously reported (Watanabe et al., 2004). RAW-D cells were plated in 100 mm plates in 10 mL of α-MEM containing 10% FBS and 1% penicillin-streptomycin. The cells were harvested when 70% confluent by pipetting without scraping to avoid activation of cells. To generate osteoclasts, cells were incubated with complete media containing 100 ng/mL RANKL, and replenished with new media every other day (without isolation). Isolation of bone-marrow macrophages (BMMs) was carried out according to a previously described method (Yamaguchi et al., 2017). Briefly, marrow cells from the femurs and tibias of mice were cultured overnight in α-MEM containing 10%

FBS in the presence of M-CSF (50 ng/mL) at 37 °C in 5% CO_2. Non-adherent cells were harvested to stroma-free bone marrow cell culture system containing 50 ng/mL M-CSF. After three days, the adherent cells were harvested as BMMs. BMMs were replated and further cultured in the presence of M-CSF (30 ng/mL) and RANKL (100 ng/mL) for 72 h.

Retrovirus construction and overexpression of abLIM1

Retrovirus construction and overexpression experiments were performed according to previously described methods (Yamaguchi et al., 2017). Briefly, the full-length cDNA of mouse abLIM1-OCL was generated by polymerase chain reaction (PCR) using cDNA derived from BMMs incubated with M-CSF and RANKL for 48 h. The cDNAs were amplified by PCR using PrimeSTAR GXL DNA polymerase (Takara, Tokyo). To express EGFP-abLIM1-OCL fusion protein, the amplified fragments were fused to a linearized pMSCVpuro-EGFP using the In-Fusion cloning kit (Clontech, Mountain View, CA, USA). A control vector was composed with only EGFP cDNA. All vectors placed EGFP at its N terminus. Vectors were transfected into HEK293T cells by using the Lipofectamine 2000 kit (Life Technologies, Gaitherburg, MD, USA), according to the manufacturer's instructions. After incubation at 37 °C in 5% CO2 for 48 h, the virus-containing supernatants were collected and used to infect RAW-D cells. abLIM1-OCL overexpressing cells were selected by puromycin (3 μg/mL) in α-MEM and every 3 days, media was removed and new media added. About 2 weeks later, several cloned cells were obtained.

Western blot analysis

Western blotting was performed according to previously described methods (Yamaguchi et al., 2017). Briefly, after washing, cells were lysed in a cell lysis buffer (50 mM Tris-HCl

[pH 8.0], 1% Nonidet P-40, 0.5% sodium deoxycholate, 0.1% SDS, 150 mM NaCl, 1 mM PMSF, and proteinase inhibitor cocktail). The same protein amounts (5 μg) were subjected to sodium dodecyl sulfate-polyacrylamide gel electrophoresis, followed by transfer onto a polyvinylidene difluoride membrane. The blots were blocked with 5% milk in Tris-buffered saline for 1 h at 25°C, incubated with various primary antibodies overnight at 4°C, washed, incubated with horseradish peroxidase-conjugated secondary antibodies, and finally detected with ECL-Prime (GE Healthcare Life Sciences, Tokyo, Japan). The immunoreactive bands were analyzed using an LAS-4000mini (Fujifilm, Tokyo, Japan).

Quantitative PCR analysis

Quantitative real-time PCR was performed according to previously described methods (Yamaguchi et al., 2017; Yoneshima et al., 2016). Total RNA was extracted using TRIzol Reagent (Invitrogen). Reverse transcription was performed using an oligo(dT)15 primer (Promega, Madison, WI, USA) and ReverTra Ace (Toyobo, Osaka, Japan). Quantitative real-time PCR was performed using a MX3005P QPCR system (Agilent Technologies, La Jolla, CA, USA). The cDNA was amplified using Brilliant III Ultra-Fast SYBR QPCR Master Mix (Agilent), according to the manufacturer's instructions. The following primer sets were used (5′ to 3′): *abLIM1*, forward: TGCTTCGCCTGTACAATCTG; and reverse: AGGACCTTCCCACAGGACTT; *TNFRS11A* (RANK), forward: CTTGGACACCTGGAATGAAGAAG; and reverse: AGGGCCTT-GCCTGCATC; *NFATC1*, forward: TCATCCTGTCCAACACCAAA and reverse: TCACCCTGGTGTTCTTCCTC;

OCSTAMP, forward: TGGGCCTCCATATGACCTCGAGTAG; and reverse:

TCAAAGGCTTGTAAATTGGAGGAGT; *DCSTAMP*, forward: CTAGCTGGCTGGACTTCATCC; and reverse: TCATGCTGTCTAGGAGACCTC; *SRC*, forward: AGAGTGCTGAGCGACCTGTGT; and reverse: GCAGAGATGCTGCCTT-GGTT; *ITGB3* (Integrin β3), forward: TGTGTGCCTGGTGCTCAGA; and reverse: AG-CAGGTTCTCCTTCAGGTTACA; *CTSK* (Cathepsin K), forward, CAGCTTCCCCAAGATGTGAT; and reverse: AGCACCAACGAGAGGAGAAA; *CALCR* (calcitonin receptor), forward: CGCATCCGCTTGAATGTG; and reverse: TCTGTCTTTCCCCAG-GAAATGA; *GAPDH*, forward: ACCACAGTCCATGCCATCAC; and reverse: TCCACCACCCTGTTGCTGTA.

Gene knockdown by siRNA

Synthetic siRNA oligonucleotide specific for abLIM1 was designed and synthesized by Invitrogen (Carlsbad, CA, USA) as follows: 5′-CCGGCACAGUUACACUCCAACUACG-3′. RAW-D cells were transfected with the siRNA oligonucleotide (20 nM/transfection), using Lipofectamine RNAiMAX (Invitrogen), according to the manufacturer's protocol. After 24 h of transfection, cells were allowed to differentiate into osteoclasts in the presence of RANKL for 4 days. Stealth siRNA Negative Control Duplexes (Invitrogen) were used as negative control.

Immunofluorescence microscopy

Immunofluorescence microscopy was performed according to previously described methods (Yamaguchi et al., 2017). Briefly, cells were fixed with 4.0% paraformaldehyde in phosphate buffered saline (PBS) for 30 min at 25 °C. After washing, the fixed cells were

permeabilized with 0.2% Triton X-100 in PBS for 15 min, and subsequently blocked with 5% normal goat serum (NGS) in PBS for 1 h, and then incubated overnight at 4 °C with anti-tubulin (1/50 dilution) or anti-actin (1/50 dilution) antibodies. After washing, the cells were stained by Alexa Fluor 488 goat anti-rabbit IgG (1/50 dilution) or Alexa Fluor 488 goat anti-rat IgG (1/50 dilution), or Alexa Fluor 546 goat anti-mouse IgG (1/50 dilution), or nuclear staining with DAPI. The samples were subjected to microscopy using a laser-scanning confocal imaging system (LSM800; Carl Zeiss, AG, Jena, Germany).

Bone resorption assay

The bone resorption activity of osteoclasts was performed using Osteo Assay Stripwell Plate (Corning) for 6 days of culture. Images for bone resorption area were taken with a CKX41 Inverted Microscope (OLYMPUS). Resorption pits were identified using ImageJ software (NIH, Bethesda, MD, USA).

Live cell imaging

Live cell imaging was performed as described previously (Iwatake et al., 2017). Briefly, images were obtained using an inverted Real-Time Cultured Cell Monitoring System CCM-1.4Z (ASTEC, Fukuoka, Japan) with a 10× objective and bright-field channels at 15-min intervals over up to 24 h for macrophage and 15-min intervals over up to 3 days for osteoclasts. Cell tracking analysis for migration was performed manually using the tracking function of the MTrackJ plugin of ImageJ.

Statistical analysis

All values were expressed as means ± standard deviation (SD) of 3 independent

experiments. The data were analyzed by the Tukey-Kramer method when analysis of variance (ANOVA) indicated a significant difference between concentrations (*$P < 0.05$ or **$P < 0.01$).

Results

Identification of a novel transcript of abLIM1 during osteoclast differentiation

Our recent study using DNA microarray analysis showed that 1,363 genes were upregulated and 881 genes were downregulated during osteoclastogenesis of bone-marrow macrophages (Shimada-Sugawara et al., 2015). Based on the data, we found the abLIM1 gene to be upregulated, as well as other osteoclast marker genes, such as calcitonin receptor, cathepsin K, carbonic anhydrase 2, and tartrate-resistant acid phosphatase (TRAP) (Fig. 1A). To confirm whether abLIM1 was upregulated during osteoclastogenesis, we tested the mRNA levels of abLIM1 during osteoclast differentiation of the murine monocytic cell line, RAW-D cells, after RANKL stimulation. Quantitative real-time PCR analysis revealed that the mRNA expression of abLIM1 was gradually increased in RANKL-stimulated RAW-D cells compared to that of unstimulated RAW-D cells (Fig. 1B). These results indicate that abLIM1expression was significantly increased during osteoclast differentiation of macrophages.

Previous studies reported that abLIM1 is expressed in various tissues as three major forms; abLIM1-L (long), abLIM1-M (middle), and abLIM1-S (short) (Roof et al., 1997) (Fig. 1C). Therefore, we examined the abLIM1 transcript(s) expressed in osteoclasts. Analysis of the PCR data and the deduced cDNA sequences revealed that the transcript of abLIM1 expressed in osteoclasts was a unique transcript, similar to abLIM1-M, and thus

termed as abLIM1-OCLs that encode LIM zinc-binding domains, coiled-coil domain, and HP domains (Fig. 1C). However, no other transcripts were detected.

Overexpression of abLIM1 suppresses multinucleation of osteoclasts

To explore the physiological roles of abLIM1 during osteoclastogenesis, we conducted overexpression experiments with a vector encoding abLIM1-OCLs-enhanced green fluorescent protein (EGFP) or EGFP alone (control) using RAW-D cells. The mRNA expression and protein levels of abLIM1-overexpressing RAW-D cells were determined by quantitative RT-PCR and western blot analyses, respectively (Fig. 2A, and B). The mRNA level of abLIM1 in abLIM1-overexpressing RAW-D cells was about 20,000-fold higher than that in control-transfected cells, since the abLIM1 expression was hardly detectable in control cells (Fig. 2A). Western blot analyses using anti-GFP and anti-abLIM1 antibodies revealed that the abLIM1-EGFP protein was detected as a major band with a molecular mass of about 90 kDa (Fig. 2B).

Under these conditions, we examined the effects of abLIM1 on osteoclastogenesis with RANKL (100 ng/mL) by TRAP staining and multinucleated cell (MNC) formation (more than 3 nuclei). TRAP staining revealed that abLIM1 overexpression abolished osteoclast differentiation upon stimulation with RANKL for 4 days (Fig. 2C). Despite detection of some TRAP-positive cells, we failed to observe MNC formation (Fig. 2 C, D). However, the viability of control and abLIM1-overexpressing osteoclasts was indistinguishable, although it was slightly increased in abLIM1-overexpressing osteoclasts (Fig. 2E).

abLIM1 overexpression reduces resorption area

We further examined bone resorption of control and abLIM1-overexpressing osteoclasts by the pit formation assay. Upon determining the resorption areas in both types, the resorption area by abLIM1-overexpressing osteoclasts was hardly detected, while that by control osteoclasts occupied approximately 3 % of the total area (Fig. 2F). The calculated data of the resorption area in both types was shown in Fig. 2G. These results indicate that the reduced resorption area is probably owing to the abolished multinucleated formation in abLIM1-overexpressing osteoclasts.

abLIM1 overexpression decreases marker gene expression of osteoclasts

To determine whether abLIM1-overexpressing osteoclasts display impaired differentiation, we measured the mRNA levels of some osteoclast-marker genes in control and abLIM1-overexpressing osteoclasts (Fig. 3). Quantitative RT-PCR analysis of 8 types of osteoclast-marker genes showed that mRNA levels of all marker genes, such as *TNFRS11R* (RANK), *NFATC1*, *OCSTAMP*, *DCSTAMP*, *SRC*, *ITGB3* (integrin β3), *CTSK* (cathepsin K) and *CALCR* (calcitonin receptor) were significantly lower in abLIM1-overexpressing osteoclasts compared to those of control cells (Fig. 3). These results suggest that expression of all osteoclast marker genes is reduced in abLIM1-overexpressing osteoclasts compared to control osteoclasts.

Differential localization of tubulin in control and abLIM1-overexpressing osteoclasts

Next, we examined the staining pattern of actin and tubulin in control and abLIM1-overexpressing osteoclasts. In control osteoclasts, EGFP was mainly detected in the cytoplasm (Fig. 4A). Staining of actin was detected along the periphery of the cells (Fig. 4A), whereas that of the tubulin was detected throughout the cytoplasm. (Fig. 4B).

However, in abLIM1-overexpressing osteoclasts, EGFP was detected along the cell periphery, which was co-localized with the actin (Fig. 4C). Staining of tubulin was also observed along with the actin, and expanding tubulin formation was not detected (Fig. 4D).

Impaired migration of abLIM1-overexpressing osteoclasts

We examined the migration of control and abLIM1-overexpressing RAW-D cells before and after stimulation with RANKL by phase-contrast microscopy. Three days after stimulation, the migration of abLIM1-overexpressing cells was decreased compared to that of control cells (Fig. 5A). The total cell migration distance and rate of abLIM1-overexpressing cells were significantly lower than those of control cells (Fig. 5B and C). These results indicate that overexpression of abLIM1 causes impaired migration of osteoclasts. The movies of migration of control and abLIM1-overexpressing RAW-D cells have also been provided (Supplement Data 1 and 2).

Knockdown of abLIM1 enhances the formation of larger and multinucleated osteoclasts

To confirm the role of abLIM1 during osteoclastogenesis, we performed knockdown experiments using siRNA transfection in RAW-D cells. We examined the knockdown efficacy of abLIM1 in RAW-D macrophages by three types of siRNAs (Fig. 6A). Depletion by siRNA #1 in the RAW-D macrophages showed approximately 50% reduction, while siRNA #2 showed approximately 70% reduction, as compared to that by control siRNA (Fig. 6A). However, siRNA #3 had no reduction activity (data not shown). Therefore, we selected siRNA #2 for following knockdown experiments. TRAP staining showed that abLIM1 knockdown resulted in the formation of remarkably larger osteoclasts upon culture

for 5 days after stimulation with RANKL (Fig. 6B). The number of TRAP-positive osteoclasts was significantly higher in abLIM1-knockdown osteoclasts than in control cells (Fig. 6C). Moreover, the nuclear number of abLIM1-knockdown osteoclasts was higher than that of control osteoclasts (Fig. 6D). Control osteoclasts containing less than 10 nuclei accounted for 90% of the total number, while those containing 11–20 nuclei accounted for 5%. However, abLIM1-knockdown osteoclasts containing more than 21–50 accounted for 8.9% of the total number, while those containing more than 51 nuclei accounted for 3% (Fig. 6D).

Similar results were observed in the native bone-marrow macrophages (BMMs). TRAP staining indicated that abLIM1-knockdown osteoclasts derived from BMMs were larger than the control osteoclasts (Fig. S1A). abLIM1-knockdown led to lower expression by approximately 60% than that of the control siRNA (Fig. S1B). The number of TRAP-positive multinucleated cells was comparable between abLIM1-depleted BMMs and control cells at three days (Fig. S1C).

abLIM1 knockdown enlarges resorption area

We further examined the bone resorption of control and abLIM1-knockdown osteoclasts by pit formation assay. Upon determining the resorption areas in both types, the resorption area by abLIM1-depleted osteoclasts was about 4-fold larger than that by control osteoclasts (Fig. 6E). The calculated data of the resorption area in both types was shown in Fig. 6F. These results indicate that the enlarged resorption area is probably due to the enhanced cell size in abLIM1-knockdown osteoclasts.

abLIM1 knockdown markedly increases marker gene expression in osteoclasts

To evaluate the differences between control and abLIM1-knockdown osteoclasts, we compared the mRNA levels of various osteoclast marker genes for both types. As shown in Fig 7, quantitative RT-PCR results showed that mRNA levels of all marker genes including *TNFRS11R* (RANK), *NFATC1*, *OCSTAMP*, *DCSTAMP*, *SRC*, *ITGB3* (integrin β3), *CTSK* (cathepsin K) and *CALCR* (calcitonin receptor) were significantly higher in abLIM1-knockdown osteoclasts compared to those in control osteoclasts. These results indicate the marked increase of marker gene expression in abLIM1-knockdown osteoclasts.

abLIM1 knockdown affects tubulin localization, migration, and fusion in osteoclasts

We further observed localization of actin and tubulin in control and abLIM1-knockdown osteoclasts (Fig. 8). abLIM1-knockdown osteoclasts displayed eccentrically located tubulin in the cytoplasm, while control osteoclasts showed moderate tubulin formation (Fig. 8B). Staining of actin was observed along the cell periphery in control and abLIM1-knockdown osteoclasts (Fig. 8A and B). However, the actin formation in abLIM1-knockdown osteoclasts was rough (Fig. 8B)., while that in control osteoclasts was smooth (Fig. 8A).

We finally monitored the migration of abLIM1-knockdown osteoclasts derived from RANKL-induced RAW-D macrophages by phase-contrast microscopy. Migration of abLIM1-depleted multinucleated cells was increased, compared with that of control cells (Fig. 9). It should be noted that multinucleation appeared in abLIM1-knockdown cells (arrow indicated), but was rare in the control cells (Fig. 9A). Both total cell migration distance and rate of abLIM1-depleted cells were significantly higher than those of control cells (Fig. 9B and C). The movies of migration of control and abLIM1-knockdown RAW-D cells have also been provided (Supplement Data 3 and 4).

Discussion

In this study, we showed an increased expression of abLIM1 during osteoclast differentiation. Overexpression of abLIM1 in RAW-D cells suppressed osteoclast differentiation compared to control cells. By contrast, knockdown of abLIM1 enhanced the formation of multinucleated osteoclasts and markedly enhanced the expression of several osteoclast marker genes. Mechanistically, abLIM1 regulated tubulin localization, migration, and fusion in osteoclasts. Thus, these results indicate that abLIM1 negatively controls osteoclast differentiation by regulating cell migration and fusion mediated via actin formation.

As unique characteristics of abLIM1, this study shows that the novel isoform abLIM-OCL was expressed in osteoclasts. So far, mouse genome analyses have revealed that there are at least 26 splicing variants at the mRNA level of mouse abLIM1 (see NCBI information Gene ID: 226251, https://www.ncbi.nlm.nih.gov/gene/226251). Among these variants, abLIM-M is ubiquitously expressed in all adult tissues at relatively high levels (Roof et al., 1997). However, in the retina, there is a photoreceptor-specific expression of the abLIM-L isoform, which contains one additional LIM cassette with abLIM-M (Roof et al., 1997). In the case of humans, abLIM1 splicing is associated with genetic disorders (Ohsawa et al., 2015). An exon 11 inclusion isoform of abLIM1 is expressed in the skeletal muscle and heart of normal individuals, but not in the skeletal muscle of patients with myotonic dystrophy type 1 (Ohsawa et al., 2015). It is likely that the tissue- or cell-specific isoforms have specialized roles in cellular processes, such as morphogenesis and differentiation. Consistent with this notion, we discovered the osteoclast-specific isoform abLIM-OCLs during osteoclast differentiation.

Both abLIM1 overexpression and knockdown experiments clearly indicate that abLIM1 negatively regulates osteoclast differentiation. Moreover, the findings demonstrated that abLIM1-overexpressing osteoclasts show abnormal tubulin formation, while abLIM1-knockdown osteoclasts show enhanced tubulin formation and increased cell migration. Several lines of evidence indicate that there is a close relationship between migration and differentiation of osteoclasts. In particular, cell-cell fusion is a critical and rate-limiting step in osteoclast differentiation (Kikuta and Ishii, 2013). Therefore, it is reasonable to speculate that rapid cell migration and aggregation mediated by abLIM1 enhance cell-cell fusion, resulting in rapid osteoclastogenesis.

So far, the physiological functions of abLIM1 in mammals are poorly understood. This is partially due to abLIM-L knockout mice displaying no phenotypes of development and maturation of retinofugal projections (Lu et al., 2003). Concerning the function of abLIM proteins, UNC115, the orthologous gene of abLIM1, has been well studied in *Caenorhabditis elegans* (Gitai et al., 2003; Lundquist et al., 1998). For example, UNC115/abLIM in *C. elegans* regulates the formation of lamellipodia and filopodia, resulting in neuronal morphogenesis (Yang and Lundquist, 2005). Recent genetic studies have shown that UNC-115/abLIM directly associates with Receptor for Activated C Kinase (RACK-1), and thereby regulation of the actin cytoskeleton and lamellipodia and filopodia formation in migrating cells (Demarco and Lundquist, 2010). Considering that RACK1 regulates osteoclast differentiation through a p38-MAPK dependent pathway (Lin et al., 2015), it is speculated that an interaction between RACK1 and abLIM1 occurs during osteoclast differentiation, thereby acting as a scaffold for the signaling modules of the actin cytoskeleton. It is of interest to determine whether abLIM1 has the same inhibitory effects as RACK1 on osteoclasts.

In conclusion, this study shows that abLIM1 negatively controls osteoclastogenesis by regulating cell migration and fusion mediated via actin formation.

Competing interests

The authors declare no competing financial interests.

Author contributions

HN, SN, and YY performed the experiments. ES, YY, MI, KO, and NY supervised data collection and analysis, TT designed the study and wrote the paper. All authors read and approved the final manuscript.

Funding

This work was supported by JSPS KAKENHI grant numbers 15H05298, 16K15790, and 17H04379

Acknowledgments

We thank Dr. Kazuhisa Nishishita for providing recombinant RANKL.

References

Boyle WJ, Simonet WS, Lacey DL. 2003. Osteoclast differentiation and activation. Nature 423(6937):337-342.

Demarco RS, Lundquist EA. 2010. RACK-1 acts with Rac GTPase signaling and UNC-115/abLIM in Caenorhabditis elegans axon pathfinding and cell migration.

PLoS genetics 6(11):e1001215.

Fiorino C, Harrison RE. 2016. E-cadherin is important for cell differentiation during osteoclastogenesis. Bone 86:106-118.

Gitai Z, Yu TW, Lundquist EA, Tessier-Lavigne M, Bargmann CI. 2003. The netrin receptor UNC-40/DCC stimulates axon attraction and outgrowth through enabled and, in parallel, Rac and UNC-115/AbLIM. Neuron 37(1):53-65.

Ishii T, Kikuta J, Kubo A, Ishii M. 2010. Control of osteoclast precursor migration: A novel point of control for osteoclastogenesis and bone homeostasis. IBMS BoneKEy 7(8):279-286.

Iwatake M, Nishishita K, Okamoto K, Tsukuba T. 2017. The Rho-Specific Guanine Nucleotide Exchange Factor Plekhg5 Modulates Cell Polarity, Adhesion, Migration, and Podosome Organization in Macrophages and Osteoclasts. Experimental cell research.

Kamiya T, Kobayashi Y, Kanaoka K, Nakashima T, Kato Y, Mizuno A, Sakai H. 1998. Fluorescence microscopic demonstration of cathepsin K activity as the major lysosomal cysteine proteinase in osteoclasts. Journal of biochemistry 123(4):752-759.

Kikuta J, Ishii M. 2013. Osteoclast migration, differentiation and function: novel therapeutic targets for rheumatic diseases. Rheumatology (Oxford, England) 52(2):226-234.

Kim AC, Peters LL, Knoll JH, Van Huffel C, Ciciotte SL, Kleyn PW, Chishti AH. 1997. Limatin (LIMAB1), an actin-binding LIM protein, maps to mouse chromosome 19 and human chromosome 10q25, a region frequently deleted in human cancers. Genomics 46(2):291-293.

Lin J, Lee D, Choi Y, Lee SY. 2015. The scaffold protein RACK1 mediates the RANKL-dependent activation of p38 MAPK in osteoclast precursors. Science signaling 8(379):ra54.

Lu C, Huang X, Ma HF, Gooley JJ, Aparacio J, Roof DJ, Chen C, Chen DF, Li T. 2003. Normal retinal development and retinofugal projections in mice lacking the retina-specific variant of actin-binding LIM domain protein. Neuroscience 120(1):121-131.

Lundberg P, Koskinen C, Baldock PA, Lothgren H, Stenberg A, Lerner UH, Oldenborg PA. 2007. Osteoclast formation is strongly reduced both in vivo and in vitro in the absence of CD47/SIRPalpha-interaction. Biochemical and biophysical research communications 352(2):444-448.

Lundquist EA, Herman RK, Shaw JE, Bargmann CI. 1998. UNC-115, a conserved protein with predicted LIM and actin-binding domains, mediates axon guidance in C. elegans. Neuron 21(2):385-392.

Ohsawa N, Koebis M, Mitsuhashi H, Nishino I, Ishiura S. 2015. ABLIM1 splicing is abnormal in skeletal muscle of patients with DM1 and regulated by MBNL, CELF and PTBP1. Genes Cells 20(2):121-134.

Roof DJ, Hayes A, Adamian M, Chishti AH, Li T. 1997. Molecular characterization of abLIM, a novel actin-binding and double zinc finger protein. The Journal of cell biology 138(3):575-588.

Sakai E, Shimada-Sugawara M, Nishishita K, Fukuma Y, Naito M, Okamoto K, Nakayama K, Tsukuba T. 2012. Suppression of RANKL-dependent heme oxygenase-1 is required for high mobility group box 1 release and osteoclastogenesis. Journal of cellular biochemistry 113(2):486-498.

Shimada-Sugawara M, Sakai E, Okamoto K, Fukuda M, Izumi T, Yoshida N, Tsukuba T. 2015. Rab27A regulates transport of cell surface receptors modulating multinucleation and lysosome-related organelles in osteoclasts. Scientific reports 5:9620.

Teitelbaum SL. 2000. Bone resorption by osteoclasts. Science (New York, NY) 289(5484):1504-1508.

Wang Y, Brooks PJ, Jang JJ, Silver AS, Arora PD, McCulloch CA, Glogauer M. 2015. Role of actin filaments in fusopod formation and osteoclastogenesis. Biochimica et biophysica acta 1853(7):1715-1724.

Watanabe T, Kukita T, Kukita A, Wada N, Toh K, Nagata K, Nomiyama H, Iijima T. 2004. Direct stimulation of osteoclastogenesis by MIP-1alpha: evidence obtained from studies using RAW264 cell clone highly responsive to RANKL. The Journal of endocrinology 180(1):193-201.

Yagi M, Miyamoto T, Sawatani Y, Iwamoto K, Hosogane N, Fujita N, Morita K, Ninomiya K, Suzuki T, Miyamoto K, Oike Y, Takeya M, Toyama Y, Suda T. 2005. DC-STAMP is essential for cell-cell fusion in osteoclasts and foreign body giant cells. The Journal of experimental medicine 202(3):345-351.

Yagi M, Miyamoto T, Toyama Y, Suda T. 2006. Role of DC-STAMP in cellular fusion of osteoclasts and macrophage giant cells. Journal of bone and mineral metabolism 24(5):355-358.

Yamaguchi Y, Sakai E, Okamoto K, Kajiya H, Okabe K, Naito M, Kadowaki T, Tsukuba T. 2017. Rab44, a novel large Rab GTPase, negatively regulates osteoclast differentiation by modulating intracellular calcium levels followed by NFATc1 activation. Cellular and molecular life sciences : CMLS.

Yang Y, Lundquist EA. 2005. The actin-binding protein UNC-115/abLIM controls formation of lamellipodia and filopodia and neuronal morphogenesis in Caenorhabditis elegans. Mol Cell Biol 25(12):5158-5170.

Yoneshima E, Okamoto K, Sakai E, Nishishita K, Yoshida N, Tsukuba T. 2016. The Transcription Factor EB (TFEB) Regulates Osteoblast Differentiation Through ATF4/CHOP-Dependent Pathway. Journal of cellular physiology 231(6):1321-1333.

Footnotes

The abbreviations used are: Actin binding LIM 1, abLIM1; receptor activator of nuclear factor kappa-B ligand, RANKL; macrophage colony-stimulating factor, M-CSF; real-time, RT; polymerase chain reaction, PCR; small interfering RNA, siRNA; alpha-minimum essential medium , α-MEM; Fetal bovine serum, FBS; tartrate-resistant acid phosphatase, TRAP; enhanced green fluorescent protein, EGFP; multinucleated cell, MNC; Receptor for Activated C Kinase, RACK-1; 6-diamidino-2-phenylindole, dihydrochloride, DAPI. bone-marrow macrophages, BMMs.

Figure Legends

Figure 1. Identification of a novel transcript of abLIM1 during osteoclast differentiation

(A) List of upregulated transcripts in rapid differentiating osteoclasts compared to slow differentiating osteoclasts. Several marker genes were described previously. (Sugawara et al.) (B) The mRNA expression of abLIM1 during osteoclast differentiation was measured by quantitative real-time PCR in RAW-D cells with 100 ng/mL RANKL. (C)

Determination of the abLIM1transcript expressed in osteoclasts. Schematic diagrams of transcripts of abLIM1.

(D) Schematic representation of mouse abLIM1 transcripts.

Figure 2. Overexpression of abLIM1 suppresses multinucleation of osteoclasts and reduces the resorption area.

RAW-D cells were transduced with either a vector containing EGFP-tagged abLIM1 or only EGFP (control).

(A) Quantitative RT-PCR analysis of abLIM1 mRNA expression levels in RAW-D cells expressing EGFP or EGFP-abLIM1. The data are represented as mean ± SD of values from five independent experiments. $^{**}P < 0.01$, compared with control cells.

(B) Western blot analysis of RAW-D cells expressing EGFP or EGFP-abLIM1. The cultured cells were harvested at day 3 and lysates were subjected to western blot analysis with anti-GFP or anti-abLIM1 antibodies.

(C) TRAP staining of control and abLIM1-overexpressing osteoclasts. Control and abLIM1-overexpressing RAW-D cells were stimulated with RANKL (100 ng/mL) for 4 days. The cells were fixed and stained for TRAP. Scale bar, 200 μm.

(D) The number of TRAP-positive MNCs in control and abLIM1 overexpressing cells was counted at the indicated day. $^{**}P < 0.01$; compared with the control cells.

(E) Cell viability of control and abLIM1-overexpressing RAW-D cells after stimulation with RANKL for 5 days. The data are represented as mean ± SD of values from five independent experiments.

(F) Bone resorption area of control and abLIM1-overexpressing osteoclasts. RAW-D cells were seeded onto Osteo Assay Stripwell Plates with RANKL (500 ng/mL) for 7 days.

Photographs of the bone resorption area of each osteoclast. Scale bar, 400 μm.

(G) The resorption area was determined using Image J software. The data are represented as mean ± SD of values from three independent experiments. $^{**}P < 0.01$, compared with control cells.

Figure 3. abLIM1 overexpression decreases marker gene expression of osteoclasts

Control and abLIM1-overexpressing RAW-D cells were cultured with RANKL (100 ng/mL) for 3 days. After isolation of mRNA, RT-PCR was performed. $^{**}P < 0.01$, compared with the control cells.

Figure 4. Differential localization of tubulin in control and abLIM1-overexpressing osteoclasts

Control and abLIM1-overexpressing RAW-D macrophages were stained with phalloidin (actin), tubulin and DAPI (blue) and analyzed by confocal microscopy. (A and B) Control RAW-D macrophages; (C and D) abLIM1-knockdown RAW-D macrophages.

Figure 5. Impaired migration of abLIM1-overexpressing RAW-D cells stimulated with RANKL

(A) Control and abLIM1-overexpressing RAW-D cells on a 6-well plate was obtained from time-lapse video microscopy. Micrographs of time-lapse imaging showing cell tracks. Representative plots of 20 cells of control and abLIM1-overexpressing RAW-D cells migration tracks for a total duration of 74 h/track. Data and pictures shown are representative of three independent experiments. (B) The distance travelled between

positions (path length). **$P < 0.01$, compared with control cells. (C) Average of migration speed of 253 samples. **$P < 0.01$, compared with control cells.

Figure 6. Knockdown of abLIM1 enhances the formation of larger and multinucleated osteoclasts and enlarges the resorption area

(A) Knockdown efficacy of abLIM1 was evaluated by measuring the mRNA levels. After incubation with RANKL (100 ng/mL) for 24 h, cells were transfected with control or abLIM1-specific siRNA (10 pmol) for an additional 24 h in the presence of RANKL. **$P <$ 0.01; compared with the control cells. **$P < 0.01$, for the indicated comparisons.

(B) TRAP staining of control and abLIM1-knockdown osteoclasts. Control and abLIM1-depleted RAW-D cells were stimulated with RANKL (100 ng/mL) for 4 days. The cells were fixed and stained for TRAP. Scale bar, 200 μm.

(C) The number of TRAP-positive MNCs in control and abLIM1-knockdown cells was counted at the indicated day. **$P < 0.01$, compared with control cells.

(D) Total nucleus number of TRAP positive multinucleated osteoclasts, but not TRAP-nega-tive mononucleated cells following a 72 h culture, was counted and classified per viewing field.

(E) Bone resorption area of control and abLIM1-knockdown osteoclasts. RAW-D cells were seeded onto Osteo Assay Stripwell Plates with RANKL (500 ng/mL) for 7 days. Photographs of the bone resorption area of each osteoclast. Scale bar, 400 μm.

(F) The resorption area was determined using Image J software. The data are represented as mean ± SD of values from three independent experiments. **$P < 0.01$, compared with control cells.

Figure 7. abLIM1 knockdown markedly increases marker gene expression in osteoclasts

Control and abLIM1-knockdown RAW-D cells were cultured with RANKL (100 ng/mL) for 3 days. After isolation of mRNA, RT-PCR was performed. $^{**}P < 0.01$, compared with control cells.

Figure 8. abLIM1 knockdown affects tubulin localization,

Control and abLIM1-knockdown RAW-D macrophages were stained with phalloidin (actin), tubulin and DAPI (blue) and analyzed by confocal microscopy. (A) Control RAW-D macrophages; (B) abLIM1-knockdown RAW-D macrophages.

Figure 9. abLIM1 knockdown enhances migration and fusion in osteoclasts

(A) Control and abLIM1-knockdown RAW-D cells seeded onto 6-well plate were analyzed by time-lapse video microscopy. Micrographs of time-lapse imaging showing cell tracks. Representative plots of 20 cells of control and abLIM1-knockdown RAW-D cells migration tracks for a total duration of 72 h/track. Data and pictures shown are representative of three independent experiments. (B) The distance travelled between positions (path length). $^{**}P < 0.01$, compared with control cells. (C) Average of migration speed of 253 samples. $^{**}P < 0.01$, compared with control cells.

Supplement Materials:

SM1: migration of control-overexpressing RAW-D cells (0~3 days)

SM2: migration of abLIM1-overexpressing RAW-D cells (0~3 days)

SM3: migration of control-knockdown RAW-D cells (0~3 days)

SM4: migration of abLIM1-knockdown RAW-D cells (0~3 days)

Supplement Figure 1:

Knockdown of abLIM1 on osteoclastogenesis of bone marrow-derived macrophages (BMMs).

(A) TRAP staining of control and abLIM1-knockdown osteoclasts. Control and abLIM1-depleted BMMs were stimulated with M-CSF (30 ng/mL) and RANKL (100 ng/mL) for 3 days. The cells were fixed and stained for TRAP. Scale bar, 200 μm.

(B) Knockdown efficacy of abLIM1 was evaluated by measuring the mRNA levels. After incubation with RANKL (100 ng/mL) for 24 h, cells were transfected with control or abLIM1-specific siRNA (10 pmol) for an additional 24 h in the presence of M-CSF and RANKL. $^{**}P < 0.01$; compared with the control cells. $^{**}P < 0.01$, for the indicated comparisons.

(C) The number of TRAP-positive MNCs in control and abLIM1-knockdown cells was counted at the indicated day. $^{**}P < 0.01$, compared with control cells.

A

Gene title	Log ratio	Reference
calcitonin receptor	3.84	Sugawara-Shimada et al.
cathepsin K	3.29	Sugawara-Shimada et al.
carbonic anhydrase 2	3.47	Sugawara-Shimada et al.
acid phosphatase 5, tartrate resistant (TRAP)	2.41	Sugawara-Shimada et al.
Actin-binding LIM protein 1	3.00	This Study

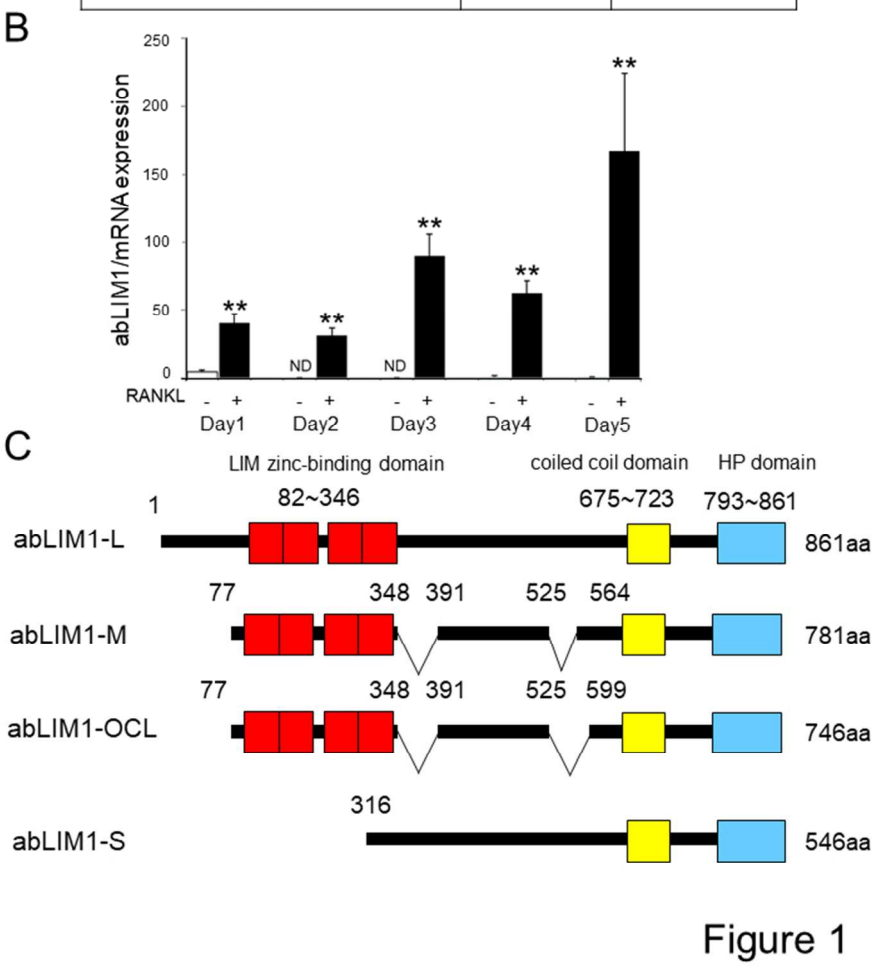

Figure 1

Fig.1

190x254mm (96 x 96 DPI)

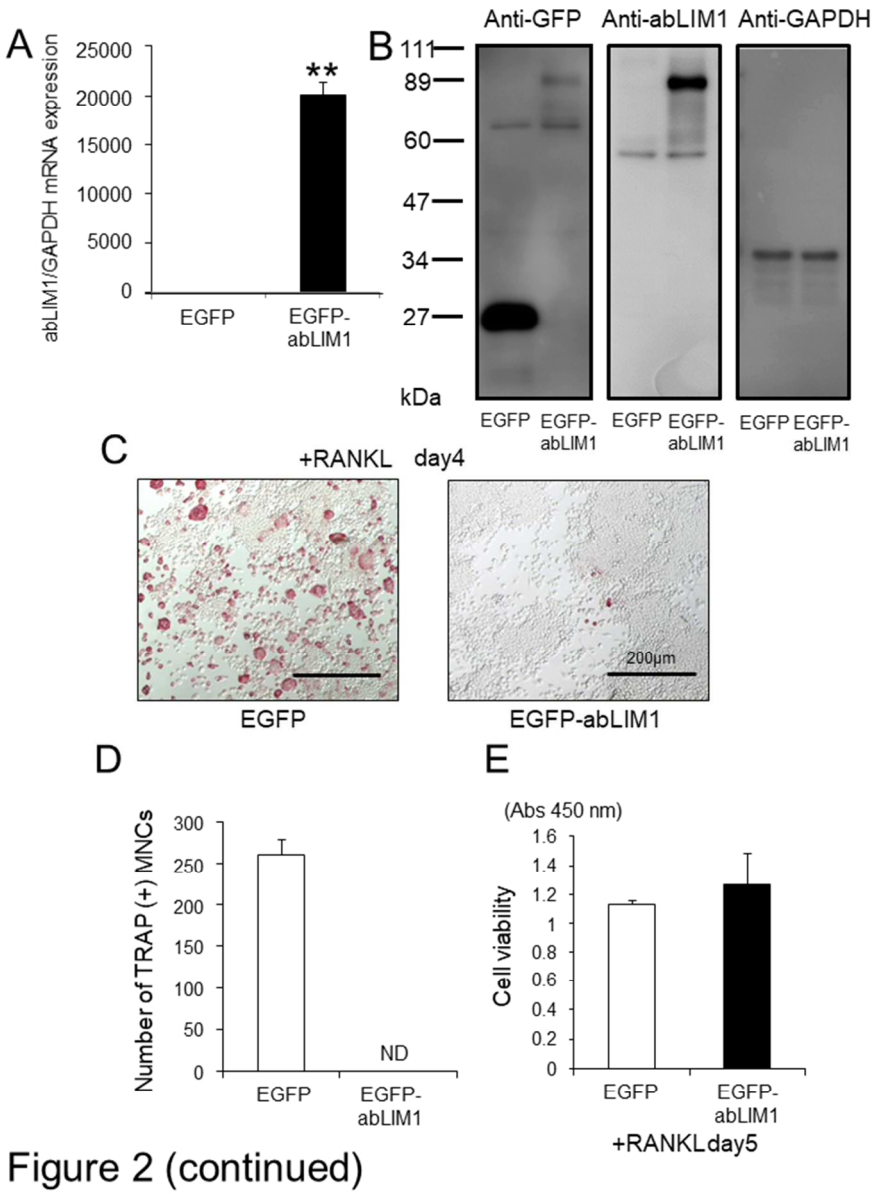

Figure 2 (continued)

Fig.2

190x254mm (96 x 96 DPI)

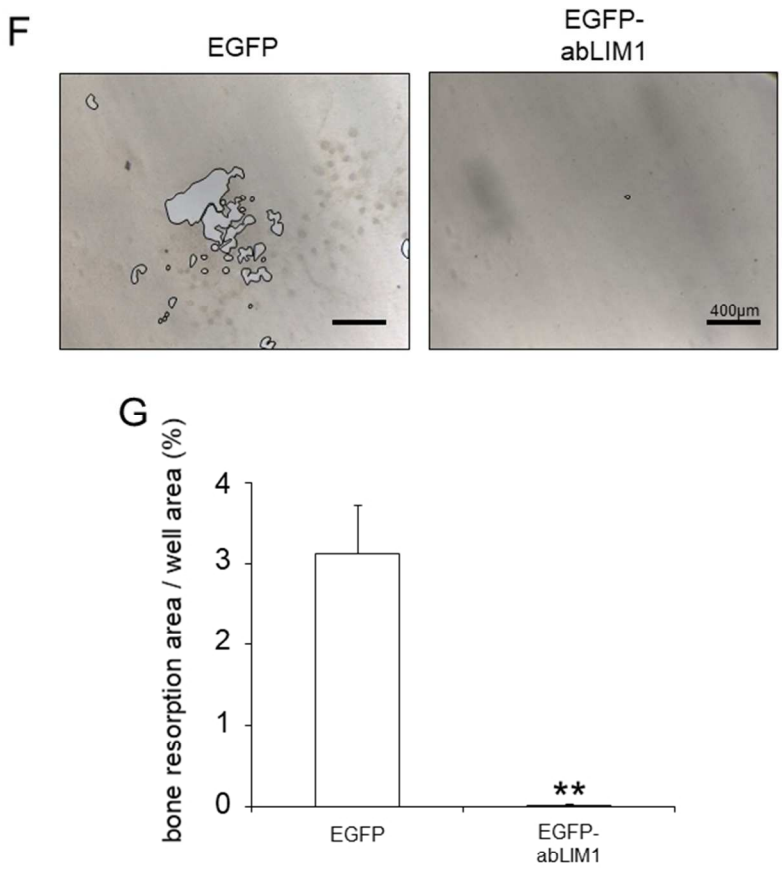

Figure 2

Fig.2

190x254mm (96 x 96 DPI)

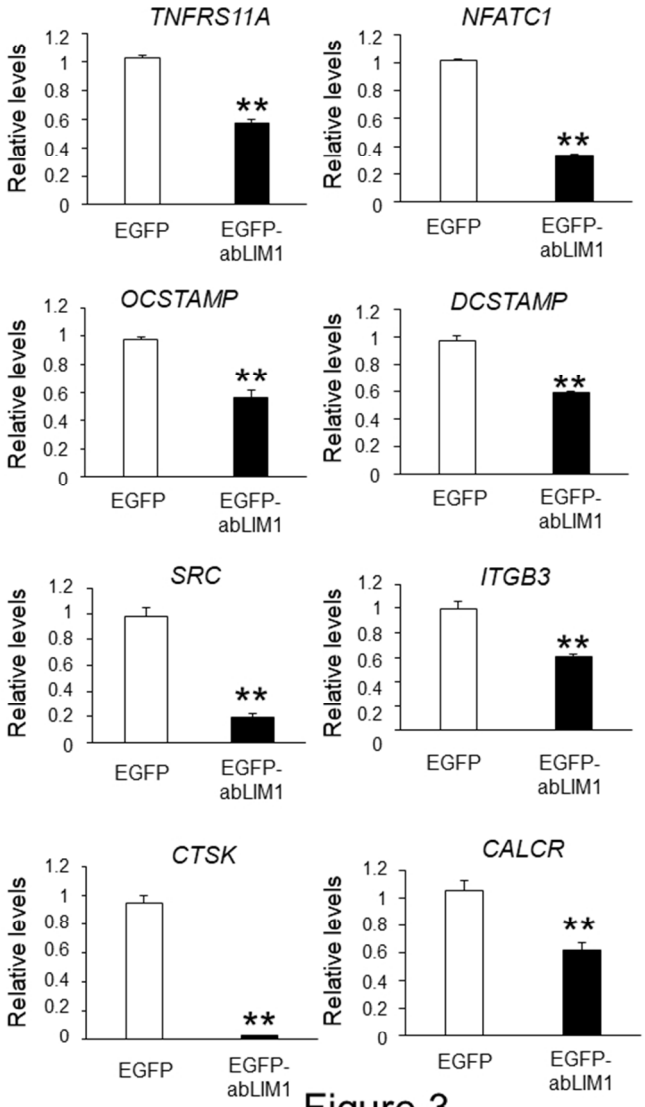

Figure 3

Fig.3

190x254mm (96 x 96 DPI)

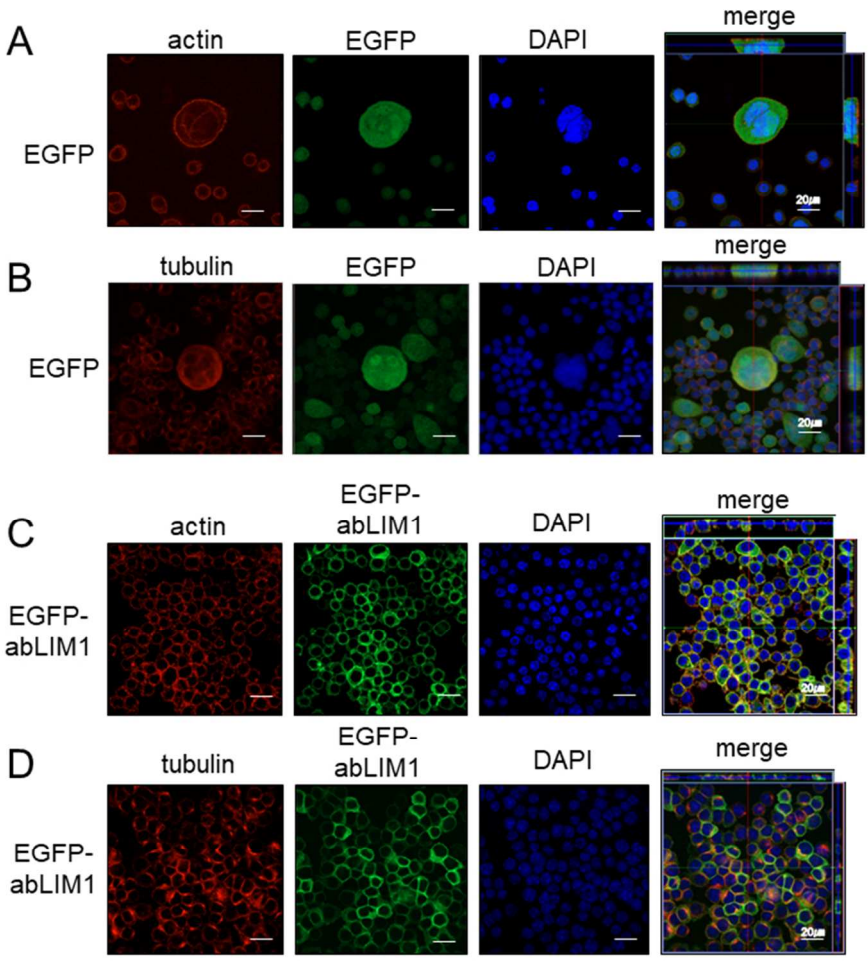

Figure 4

Fig.4

190x254mm (96 x 96 DPI)

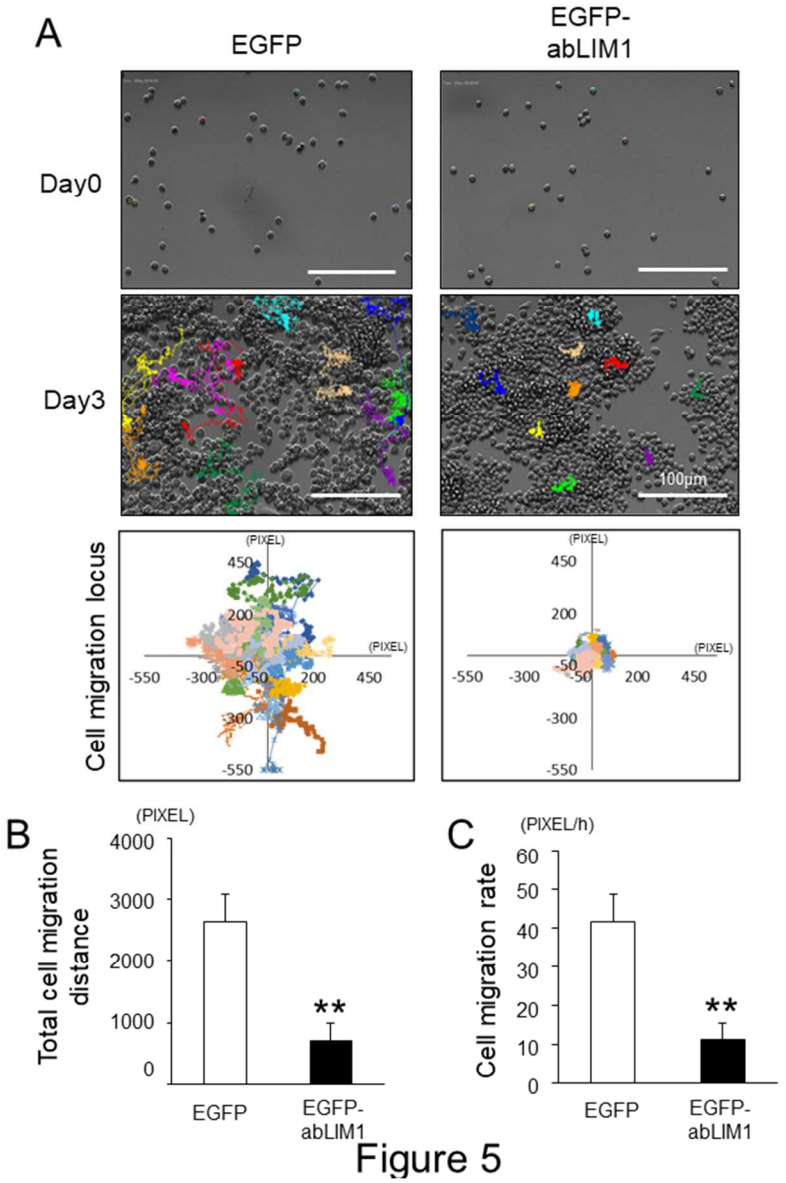

Figure 5

Fig.5

190x254mm (96 x 96 DPI)

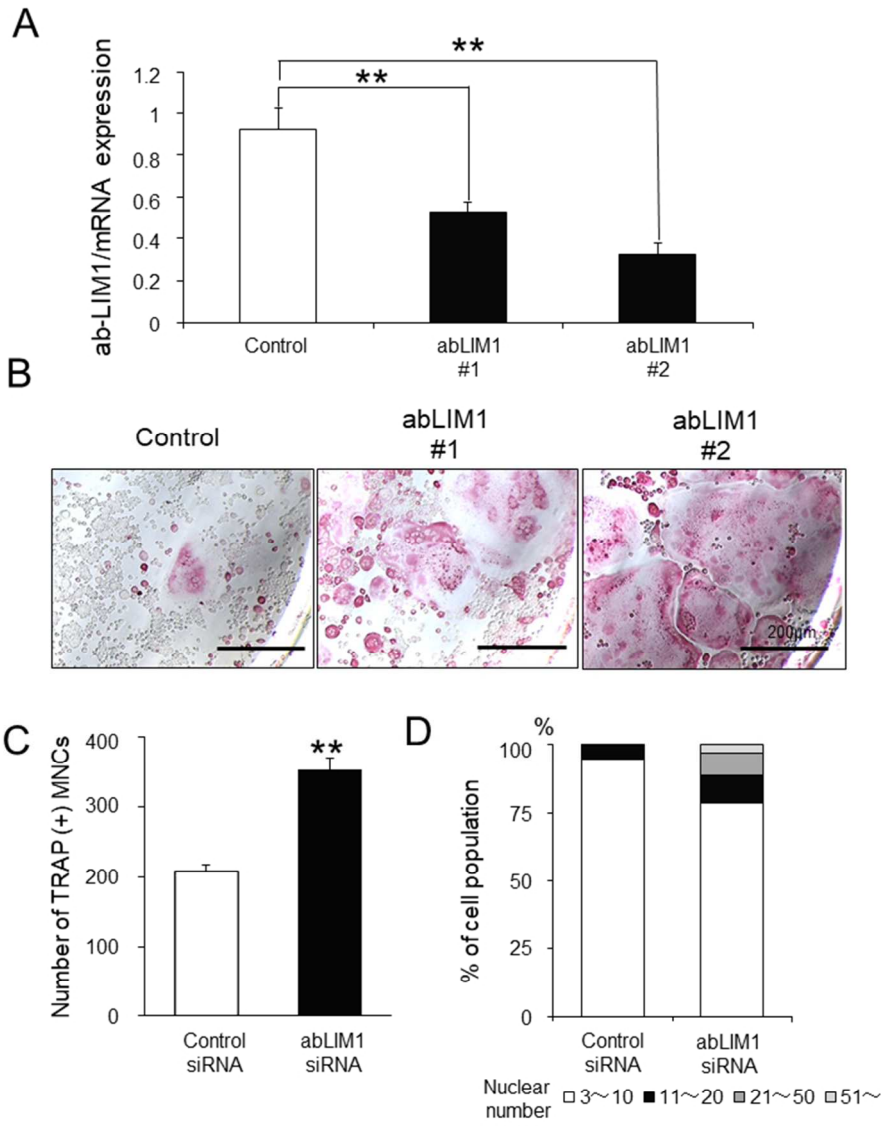

Figure 6 (continued)

Fig.6

190x254mm (96 x 96 DPI)

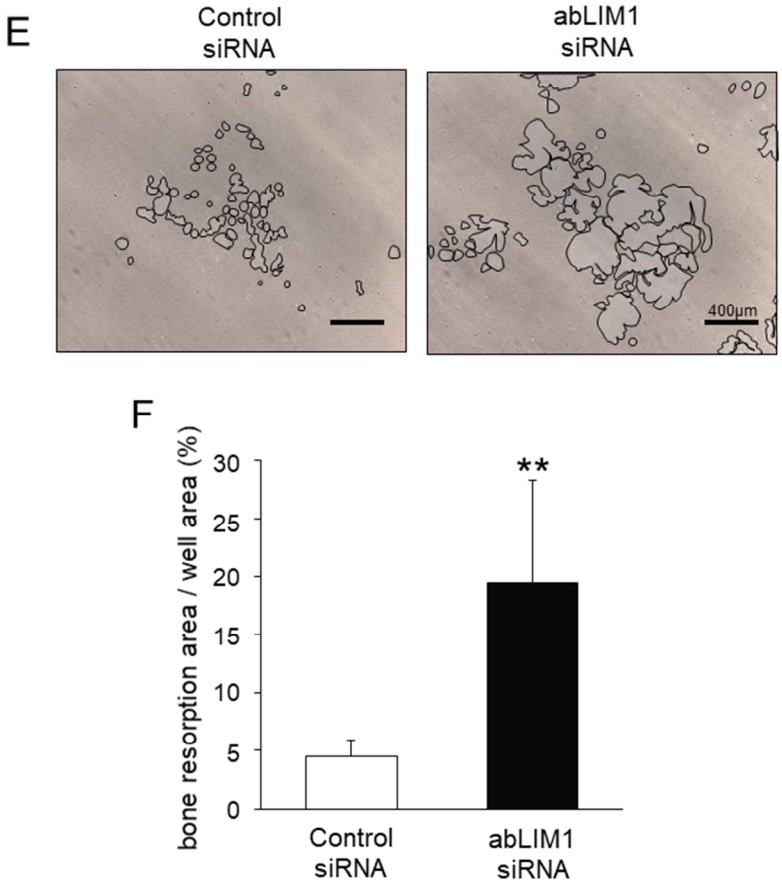

Figure 6

Fig.6

190x254mm (96 x 96 DPI)

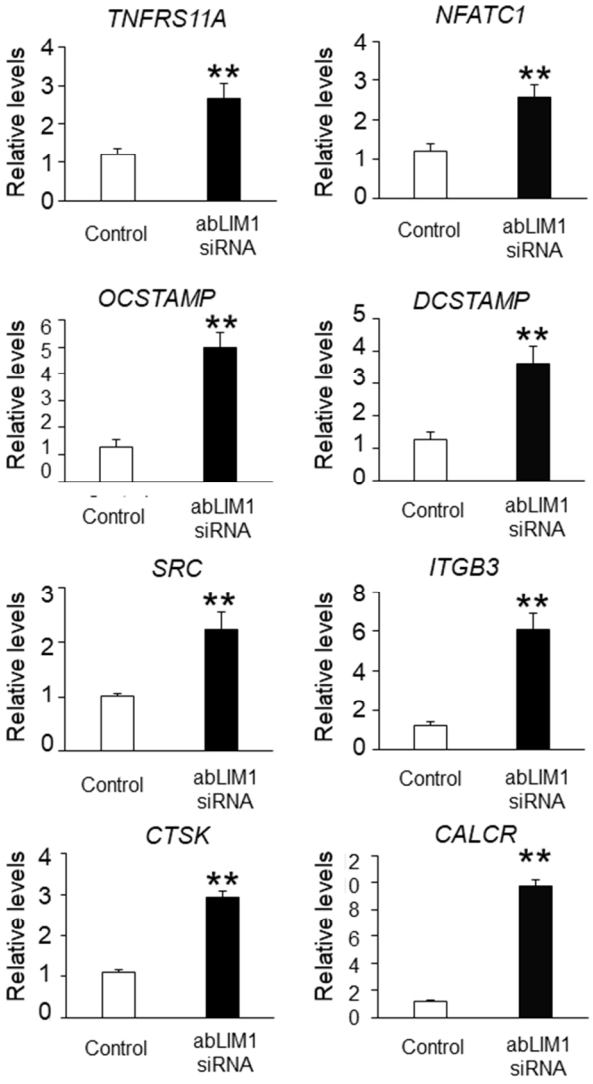

Figure 7

Fig.7

190x254mm (96 x 96 DPI)

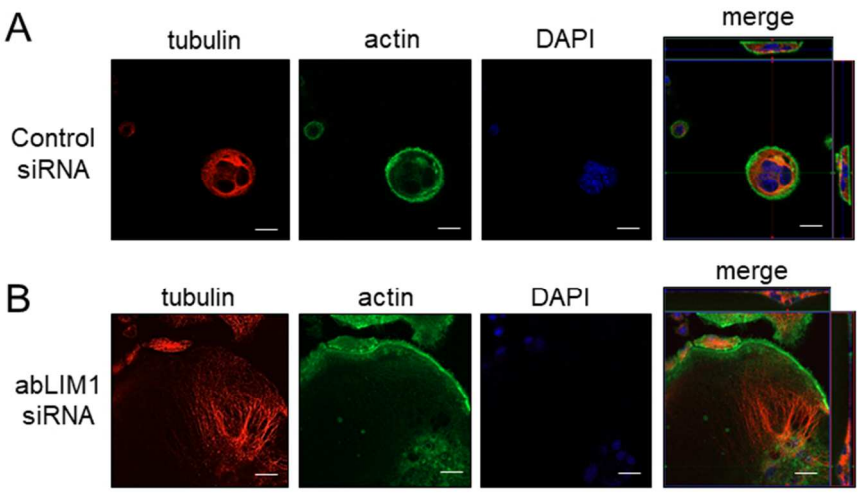

Figure 8

Fig.8

190x254mm (96 x 96 DPI)

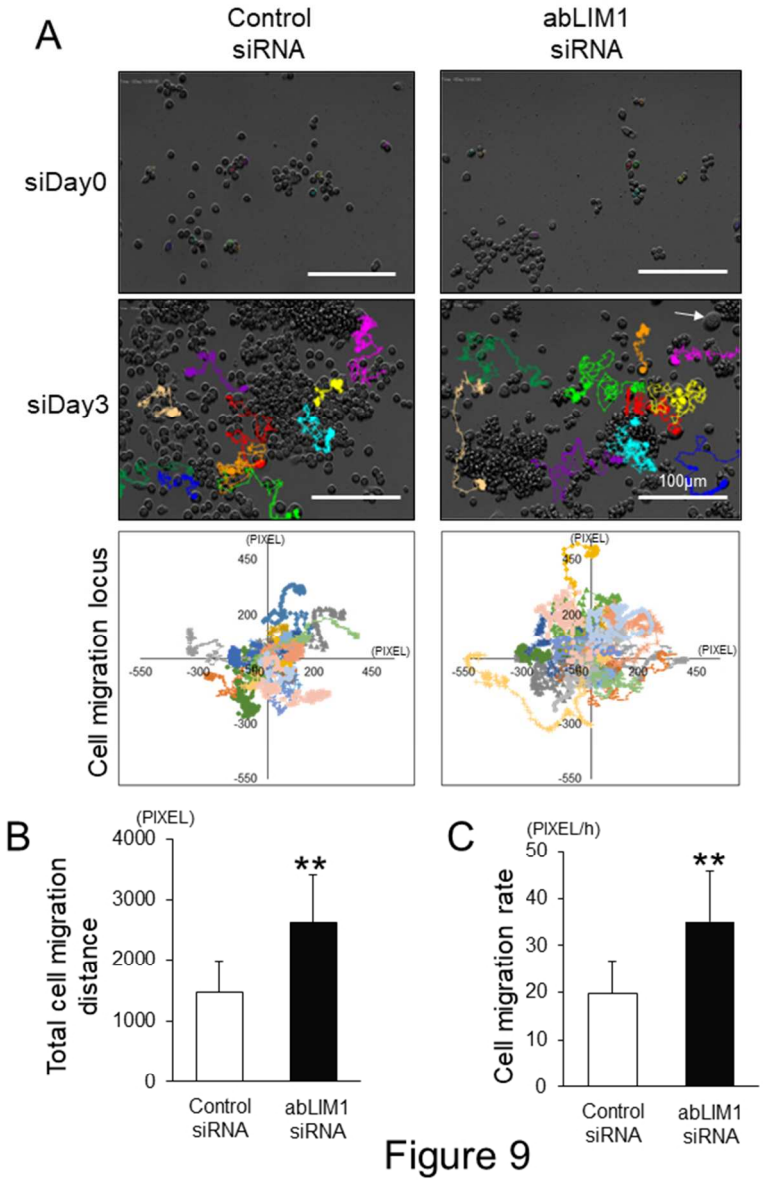

Figure 9

Fig.9

190x254mm (96 x 96 DPI)